

Eugene L. Starostin and Gert H.M. van der Heijden
Equilibria of elastic cable knots and links

Abstract: We present a theory for equilibria of geometrically exact braids made of two thin, uniform, homogeneous, isotropic, initially-straight, inextensible and unshearable elastic rods of circular cross-section. We formulate a second-order variational problem for an action functional whose Euler–Lagrange equations, partly in Euler–Poincaré form, yield a compact system of ODEs for which we define boundary-value problems for braids closed into knots or links. The purpose of the chapter is to present a pathway of deformations leading to braids with a knotted axis, thereby offering a way to systematically compute elastic cable knots and links. A representative bifurcation diagram and selected numerical solutions illustrate our approach.

Keywords: elastic knots and links, cable knots, equilibria, variational problem, bifurcation

MSC: 74K10, 74G60, 65L10


12.1 Introduction

Contact problems in the theory of elasticity have seen a surge of interest recently. They are challenging because of the one-sided constraints they introduce. Determining the topology and geometry of the contact set given the boundary conditions is probably the hardest part of any contact problem. Although progress has been made in some of the 1D continua problems [8], [5], [13], we are still far from a full understanding of the solutions of the Euler–Lagrange equations for general contact problems. The theory of elastic braids in [12] deals with a special type of (self-)contact problems of elastic rods involving only equality constraints.

In this work we focus our attention on closed braids whose axes make a torus knot, i.e., so-called cable knots or links [2]. Such knots or links form naturally in (virtual) experiments with elastic torus knots/links if they are made to buckle under the insertion of twist and then allowed to go through a (multiple) self-intersection (the simplest example being the passage through a figure-8 with a single self-intersection). We do not intend to present in this chapter a global classification of all equilibria of knotted 2-braids; rather we explain a particular scenario of how they appear in a typical bifurcation diagram as a control parameter (such as the twisting moment) is varied. We make no assumptions on either the topology or the geometry of the contact set ex-

Eugene L. Starostin, Gert H.M. van der Heijden, Department of Civil, Environmental & Geomatic Engineering, University College London, Gower Street, London WC1E 6BT, United Kingdom, E-mails: e.starostin@ucl.ac.uk, g.heijden@ucl.ac.uk

<https://doi.org/10.1515/9783110571493-011>

Open Access.  © 2018 Eugene L. Starostin and Gert H.M. van der Heijden, published by De Gruyter. This work is licensed under the Creative Commons Attribution-NonCommercial-NoDerivs 4.0 License.

cept that it is closed on itself. We obtain the shape of the contact curve as part of the solution.

In Section 2 we first recall the essential equations of the elastic 2-braid theory [12] specialised to the present case of $(n, 2)$ -cable knots/links. Then, in Section 3, we formulate boundary conditions that smoothly seal the ends of the rods so that a knot or a link is formed and discuss a bifurcation diagram and numerical solutions before closing this study, in Section 4, with some concluding remarks.

12.2 Theory of elastic braids made of two equidistant strands

12.2.1 Equidistant curves, reference frames and strains

Consider a pair of smooth curves $\mathbf{r}_1(s) \in \mathbb{R}^3$, $s \in [0, L_1]$, $\mathbf{r}_2(\sigma) \in \mathbb{R}^3$, $\sigma \in [0, L_2]$, both parametrised by arclength, that serve as centrelines of two inextensible and unsharable elastic rods of length $L := L_1$ and L_2 , respectively. We denote by $\mathbf{t}_1(s) = \frac{d\mathbf{r}_1(s)}{ds}$ and $\mathbf{t}_2(\sigma) = \frac{d\mathbf{r}_2(\sigma)}{d\sigma}$ the unit tangents to each of the curves. We define the point-to-point squared distance function $D_2(s, \sigma) = \boldsymbol{\rho}^2(s, \sigma)$, where $\boldsymbol{\rho}(s, \sigma) = \mathbf{r}_2(\sigma) - \mathbf{r}_1(s)$ is a chord vector connecting the two curves. We assume that there is a one-to-one mapping $[0, L_1] \leftrightarrow [0, L_2] : s \leftrightarrow \sigma(s)$ between the two curves such that D_2 is bi-critical at corresponding points, i.e., $\frac{\partial D_2}{\partial s}(s, \sigma) \Big|_{\sigma=\sigma(s)} = -2\boldsymbol{\rho}(s, \sigma(s)) \cdot \mathbf{t}_1(s) = 0$ and $\frac{\partial D_2}{\partial \sigma}(s, \sigma) \Big|_{\sigma=\sigma(s)} = 2\boldsymbol{\rho}(s, \sigma(s)) \cdot \mathbf{t}_2(\sigma(s)) = 0$. Then $D_2(s, \sigma(s))$ is constant, say equal to Δ^2 , and the two curves are said to be at constant distance Δ . Moreover the chords $\boldsymbol{\rho}(s, \sigma(s))$ are orthogonal to the curve tangents at both ends. Because of the one-to-one mapping there exists a common parametrisation for both curves. Taking arclength along the first curve as the common parameter, we can introduce the unit chord vector $\mathbf{d}_1(s) = \frac{1}{\Delta}\boldsymbol{\rho}(s, \sigma(s)) = \frac{1}{\Delta}[\mathbf{r}_2(\sigma(s)) - \mathbf{r}_1(s)]$. We shall henceforth write expressions like $\mathbf{r}_2(s)$ instead of $\mathbf{r}_2(\sigma(s))$.

Along each curve we define two moving frames as follows (Fig. 12.1). We define $\mathbf{u}_1 := \mathbf{t}_1 \times \mathbf{d}_1$ so that the vectors \mathbf{t}_1 , \mathbf{d}_1 and \mathbf{u}_1 form an orthonormal frame that we call the first braid frame. We also define an orthonormal material frame on the first rod: $\{\mathbf{t}_1, \mathbf{d}_0, \mathbf{v}_1\}$ (\mathbf{d}_0 pointing in an arbitrary normal direction). The two frames differ by a rotation about \mathbf{t}_1 through an angle ξ_1 measured from \mathbf{d}_0 to \mathbf{d}_1 . Correspondingly, we define two moving orthonormal frames on the second curve \mathbf{r}_2 . The first one (called the second braid frame) is made up of the vectors \mathbf{t}_2 , \mathbf{d}_1 and $\mathbf{u}_2 := \mathbf{t}_2 \times \mathbf{d}_1$, while the second one (called the second material frame) is $\{\mathbf{t}_2, \mathbf{d}_2, \mathbf{v}_2\}$. They differ by a rotation about the tangent vector \mathbf{t}_2 through an angle ξ_2 , measured from \mathbf{d}_1 to \mathbf{d}_2 .

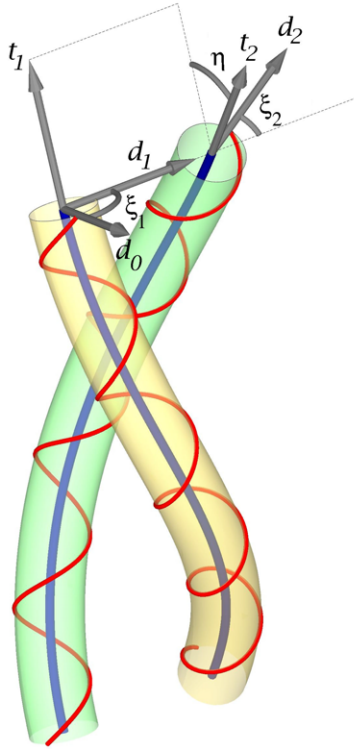


Fig. 12.1: A braid made of two rods. Centrelines are drawn as thick blue curves while red helices show how the material twists. For clarity the rods are shown with smaller diameter.

After choosing a coordinate system we may identify the orientations of the above four reference frames with elements of the group of orthogonal 3×3 matrices:

$$R_{ij}(s) := (\mathbf{t}_j(s), \mathbf{d}_i(s), \boldsymbol{\beta}_{ij}(s)) \in SO(3),$$

$$\boldsymbol{\beta}_{ij}(s) = \mathbf{t}_j(s) \times \mathbf{d}_i(s) = i(2 - i)\mathbf{u}_j(s) + |i - 1|\mathbf{v}_j(s),$$

where $i \in \{0, 1, 2\}$, $j \in \{1, 2\}$, $ij \neq 02, 21$. These define four skew-symmetric 3×3 matrices in the Lie algebra $\mathfrak{so}(3)$ as follows:

$$\widehat{\omega} = R_{11}^T R'_{11}, \quad \widehat{\Omega} = R_{12}^T R'_{12}, \quad \widehat{\omega} = R_{01}^T R'_{01}, \quad \widehat{\Omega} = R_{22}^T R'_{22}, \quad (12.2.1)$$

where we have introduced the ‘hat’ isomorphism between skew-symmetric matrices

$$\widehat{w} = \begin{pmatrix} 0 & -w_3 & w_2 \\ w_3 & 0 & -w_1 \\ -w_2 & w_1 & 0 \end{pmatrix} \text{ in } \mathfrak{so}(3) \text{ and axial (rotation) vectors } w = (w_1, w_2, w_3)^T \text{ in}$$

\mathbb{R}^3 .^{12.1} Here and in the following a prime denotes differentiation with respect to s . Thus we have defined four axial vectors $\omega = (\omega_1, \omega_2, \omega_3)^\top$, $\Omega = (\Omega_1, \Omega_2, \Omega_3)^\top$, $\tilde{\omega} = (\tilde{\omega}_1, \tilde{\omega}_2, \tilde{\omega}_3)^\top$ and $\tilde{\Omega} = (\tilde{\Omega}_1, \tilde{\Omega}_2, \tilde{\Omega}_3)^\top$, which are the rotation vectors of, respectively, the braid frames $\{\mathbf{t}_1, \mathbf{d}_1, \mathbf{u}_1\}$, $\{\mathbf{t}_2, \mathbf{d}_1, \mathbf{u}_2\}$ and the material frames $\{\mathbf{t}_1, \mathbf{d}_0, \mathbf{v}_1\}$ and $\{\mathbf{t}_2, \mathbf{d}_2, \mathbf{v}_2\}$.

The orthonormal frames form a sequence under consecutive rotations about \mathbf{t}_1 , \mathbf{d}_1 and \mathbf{t}_2 . Thus

$$R_{11} = R_{01}R_1(\xi_1), \quad R_{12} = R_{11}R_2(\eta), \quad R_{22} = R_{12}R_1(\xi_2), \quad (12.2.2)$$

where

$$R_1(\xi_i) = \exp(\xi_i \hat{e}_1) = \begin{pmatrix} 1 & 0 & 0 \\ 0 & \cos \xi_i & -\sin \xi_i \\ 0 & \sin \xi_i & \cos \xi_i \end{pmatrix} \in SO(3), \quad i = 1, 2, \quad e_1 = (1, 0, 0)^\top,$$

$$R_2(\eta) = \exp(\eta \hat{e}_2) = \begin{pmatrix} \cos \eta & 0 & \sin \eta \\ 0 & 1 & 0 \\ -\sin \eta & 0 & \cos \eta \end{pmatrix} \in SO(3), \quad e_2 = (0, 1, 0)^\top,$$

and η is the angle, about \mathbf{d}_1 , from the first tangent, \mathbf{t}_1 , to the second, \mathbf{t}_2 (see Fig. 12.1). From Eqs. (12.2.1), (12.2.2) it follows that the rotation vectors of the material and braid frames are related as

$$\hat{\omega} = R_1^\top(\xi_1)\hat{\tilde{\omega}}R_1(\xi_1) + R_1^\top(\xi_1)R_1'(\xi_1), \quad (12.2.3)$$

$$\hat{\Omega} = R_2^\top(\eta)\hat{\omega}R_2(\eta) + R_2^\top(\eta)R_2'(\eta), \quad (12.2.4)$$

$$\hat{\tilde{\Omega}} = R_1^\top(\xi_2)\hat{\Omega}R_1(\xi_2) + R_1^\top(\xi_2)R_1'(\xi_2). \quad (12.2.5)$$

Owing to the inextensibility condition $|\frac{dr_2}{d\sigma}| = 1$, the arclength parameter σ along the second centreline satisfies

$$\sigma' = \sqrt{(\Delta\omega_1)^2 + (\Delta\omega_3 - 1)^2}. \quad (12.2.6)$$

We express the angle η as a function of the components of ω as

$$\sin \eta = -\Delta\omega_1/\sigma', \quad \cos \eta = (1 - \Delta\omega_3)/\sigma', \quad (12.2.7)$$

and hence

$$\omega_1 = \left(\omega_3 - \frac{1}{\Delta} \right) \tan \eta. \quad (12.2.8)$$

12.1 Throughout we adopt the notation that for any vector $\mathbf{v} \in \mathbb{R}^3$ the sans-serif symbol v denotes the triple of components $(v_1, v_2, v_3)^\top = (\mathbf{v} \cdot \mathbf{t}_1, \mathbf{v} \cdot \mathbf{d}_1, \mathbf{v} \cdot \mathbf{u}_1)^\top$ in the first braid frame. An exception is however made for sans-serif rotation vectors, which are always triples of components in their corresponding frames.

Eqs. (12.2.3)–(12.2.5) allow us to express the strand strains $(\tilde{\omega}_1, \tilde{\omega}_2, \tilde{\omega}_3, \tilde{\Omega}_1, \tilde{\Omega}_2, \tilde{\Omega}_3)$ in terms of the variables $(\omega_1, \omega_2, \omega_3, \xi_1, \xi_2)$, which we shall call the braid strains. In much of the following it will be convenient to use Eq. (12.2.8) to eliminate ω_1 in favour of the angle η , which also has an intuitive physical meaning as braid angle. With either choice of variables we have an unconstrained description in which, by construction, the constant-distance constraint is automatically satisfied.

We note that if $\omega_1 = 0$ and $\omega_3 \neq 1/\Delta$, then $\eta = 0$ and the two strands are parallel (this condition does not restrict in any way the shape of the first centreline). When $\omega_3 = 1/\Delta$, and $\omega_1 \neq 0$, the second strand becomes orthogonal to the first one ($\eta = \pm\pi/2$). If both $\omega_1 = 0$ and $\omega_3 = 1/\Delta$ then $\sigma' = 0$, i.e., the induced parametrisation of the second centreline is singular. The angle η is then not defined. We need to rule out this case.

For a non-selfintersecting braid, tubes of radius $\Delta/2$ around each of the centrelines must not overlap. Locally this means that points connected by the bicritical chords must be closest-approach points of the centrelines. It may be shown that this requires $\eta \in (-\pi/2, \pi/2)$ [12].

12.2.2 Equations for the standard 2-braid

For the elastic energy we make the usual assumption of frame indifference, i.e., the energy is invariant under Euclidean motions. It will then depend only on the strains (and possibly arclength) and not, for instance, on the centreline \mathbf{r}_1 . We have already assumed both rods in the braid to be inextensible and unsharable, so there is no elastic energy on account of stretches. Apart from this restriction we allow for arbitrary hyperelastic rods [1] and write

$$U_1 = \int_0^{L_1} f_1(\tilde{\omega}) \, ds \quad \text{and} \quad U_2 = \int_0^{L_2} f_2(\tilde{\Omega}(\sigma)) \, d\sigma = \int_0^{L_1} f_2(\tilde{\Omega}/\sigma') \sigma' \, ds \quad (12.2.9)$$

for the elastic strain energy of the first and second rod, respectively, where f_1 and f_2 are the strand strain energy densities, and the explicit argument of $\tilde{\Omega}$ in the σ integral emphasises that $\tilde{\Omega}$ is to be regarded as a function of arclength σ of the second rod in this integral.

Assuming fixed ends of the first strand, we add $-\mathbf{F} \cdot [\mathbf{r}_1(L) - \mathbf{r}_1(0)] = -\int_0^L \mathbf{F} \cdot \mathbf{t}_1 \, ds$ as an isoperimetric constraint expression with \mathbf{F} a (constant) Lagrange multiplier (to become the internal force in the braid). Also, by inextensibility of the second rod we require the length of the second strand

$$L_2 = \int_0^{L_2} d\sigma = \int_0^L \sigma' \, ds =: \int_0^L f_\sigma(\omega_1, \omega_3) \, ds \quad (12.2.10)$$

to be constant, giving a second isoperimetric constraint.

We can express the arguments of the integrands in Eqs. (12.2.9) and (12.2.10) in terms of the braid strains (ω, ξ_1, ξ_2) and their derivatives by using Eqs. (12.2.3)–(12.2.5) and (12.2.6) and thus formulate a second-order variational problem for the reduced functional $l : 2\text{so}(3) \times \mathbb{R}^3 \times TS^1 \times TS^1 \rightarrow \mathbb{R}$, $l(\omega, \omega', F, \xi_1, \xi_1', \xi_2, \xi_2') = f_1(\tilde{\omega}) + f_2(\tilde{\Omega}(\sigma)) + h\sigma' - F \cdot t_1$,

$$\delta \int_0^L l(\omega, \omega', F, \xi_1, \xi_1', \xi_2, \xi_2') ds = 0, \quad (12.2.11)$$

for variations that keep the end positions and orientations of the rods fixed; h is a (constant) Lagrange multiplier.

The Euler–Lagrange equations are derived partly in Euler–Poincaré form and comprise

- (a) balance equations for the components of the overall braid force $F = (F_1, F_2, F_3)^\top$ and braid moment $M = (M_1, M_2, M_3)^\top$ expressed in the first braid frame [12]

$$F' + \omega \times F = 0, \quad (12.2.12)$$

$$M' + \omega \times M + t_1 \times F = 0, \quad (12.2.13)$$

- (b) the ‘constitutive’ equations

$$M = \mathcal{E}_\omega(l), \quad (12.2.14)$$

where $\mathcal{E}_\zeta(k) := \frac{\partial k}{\partial \zeta} - \left(\frac{\partial k}{\partial \zeta'} \right)'$ is the Euler-Lagrange operator for the variable ζ ,

- (c) the phase equations for the twist angles of the rods

$$\mathcal{E}_{\xi_i}(l) = 0, \quad i = 1, 2. \quad (12.2.15)$$

Equations (12.2.12) and (12.2.13) are the moving-frame (advected) versions of the familiar balance equations $F' = \mathbf{0}$, $M' + r_1' \times F = \mathbf{0}$ expressed in an inertial frame. It follows that $|F|$ and $F \cdot M$ are first integrals.

Equations (12.2.15) can be written as a set of four first-order equations by introducing new variables (the strand torques) T_i , $i = 1, 2$:

$$T_i = \frac{\partial l}{\partial \xi_i'}, \quad T_i' = \frac{\partial l}{\partial \xi_i}. \quad (12.2.16)$$

If we eliminate the variable ω_1 in favour of η by using $\eta = \eta(\omega_1, \omega_3)$ given in Eq. (12.2.7), the reduced density l takes the form

$$l = g(\omega_2, \omega_3, \eta, \eta', F_1, \xi_1, \xi_1', \xi_2, \xi_2'), \quad (12.2.17)$$

while Eq. (12.2.14) transforms into [11]

$$M_1 = \frac{\partial \eta}{\partial \omega_1} \varepsilon_\eta(\mathbf{g}) = \frac{\Delta \cos^2 \eta}{\Delta \omega_3 - 1} \left[\frac{\partial \mathbf{g}}{\partial \eta} - \frac{d}{ds} \left(\frac{\partial \mathbf{g}}{\partial \eta'} \right) \right], \quad (12.2.18)$$

$$M_2 = \frac{\partial \mathbf{g}}{\partial \omega_2}, \quad (12.2.19)$$

$$M_3 = \frac{\partial \mathbf{g}}{\partial \omega_3} + \frac{\partial \eta}{\partial \omega_3} \varepsilon_\eta(\mathbf{g}) = \frac{\partial \mathbf{g}}{\partial \omega_3} - \frac{\Delta \sin \eta \cos \eta}{\Delta \omega_3 - 1} \left[\frac{\partial \mathbf{g}}{\partial \eta} - \frac{d}{ds} \left(\frac{\partial \mathbf{g}}{\partial \eta'} \right) \right] \quad (12.2.20)$$

(cf. the equations for an elastic strip reduced to the centreline in [10]).

We now specialise our theory to the case where the two strands are linearly elastic, uniform, isotropic, initially-straight rods with bending stiffness B_1 and B_2 and torsional stiffness C_1 and C_2 , respectively. We allow the strands to be intrinsically twisted with twist rates ω_{01} and ω_{02} . We call this special case the standard 2-braid. The density g in Eq. (12.2.17) then takes the form

$$g = g_e(\omega_2, \omega_3, \eta, \eta', \xi'_1, \xi'_2) + h(1 - \Delta \omega_3) / \cos \eta - F_1, \quad (12.2.21)$$

with the elastic energy density $g_e (= f_1 + f_2)$, the sum of bending and torsional energy densities of the two strands, given by (using Eqs. (12.2.3)–(12.2.5))

$$\begin{aligned} g_e &= \frac{1}{2} \left[B_1(\tilde{\omega}_2^2 + \tilde{\omega}_3^2) + \frac{B_2}{\sigma'}(\tilde{\Omega}_2^2 + \tilde{\Omega}_3^2) + C_1(\tilde{\omega}_1 - \omega_{01})^2 + \frac{C_2}{\sigma'}(\tilde{\Omega}_1 - \sigma' \omega_{02})^2 \right] = \\ &= \frac{1}{2} \left\{ B_1(\omega_2^2 + \omega_3^2) + B_2 \left[\frac{\cos \eta}{1 - \Delta \omega_3} (\omega_2 + \eta')^2 + \frac{(\omega_3 - \sin^2 \eta / \Delta)^2}{(1 - \Delta \omega_3) \cos \eta} \right] + \right. \\ &\quad \left. + C_1 \left[\left(\omega_3 - \frac{1}{\Delta} \right) \tan \eta - \xi'_1 - \omega_{01} \right]^2 + \right. \\ &\quad \left. + C_2 \left[\frac{\cos \eta}{1 - \Delta \omega_3} \left(\frac{\sin \eta}{\Delta} - \xi'_2 \right)^2 + 2\omega_{02} \left(\frac{\sin \eta}{\Delta} - \xi'_2 \right) + \omega_{02}^2 \frac{1 - \Delta \omega_3}{\cos \eta} \right] \right\}. \quad (12.2.22) \end{aligned}$$

This gives a system of 13 ODEs in $(F_1, F_2, F_3, M_1, M_2, M_3, \eta, \omega_2, \omega_3, \xi_1, T_1, \xi_2, T_2)$: Eqs. (12.2.12), (12.2.13), (12.2.16), (12.2.18), (12.2.19) and (12.2.20). The last three in fact contain two algebraic equations because g does not depend on ω'_2 and ω'_3 , but these can be turned into ODEs by differentiation (and the algebraic equations used to solve for η' and h). Also note that since g does not depend on the phase angles ξ_1 and ξ_2 , the strand torques T_i are constants.

12.2.3 Kinematics equations

Reconstruction of the centreline of the first strand requires solving for the tangent \mathbf{t}_1 and integrating this to get \mathbf{r}_1 . We choose a parametrisation of the first braid frame $\{\mathbf{t}_1, \mathbf{d}_1, \mathbf{u}_1\}$ in terms of four Euler parameters (or quaternions) $\mathbf{q} = (q_0, q_1, q_2, q_3)$ subject

to the normalisation condition $q_0^2 + q_1^2 + q_2^2 + q_3^2 = 1$ [6] and write

$$\mathbf{t}_1 = \begin{pmatrix} q_0^2 + q_1^2 - q_2^2 - q_3^2 \\ 2q_1q_2 + 2q_0q_3 \\ 2q_1q_3 - 2q_0q_2 \end{pmatrix}, \quad \mathbf{d}_1 = \begin{pmatrix} 2q_1q_2 - 2q_0q_3 \\ q_0^2 - q_1^2 + q_2^2 - q_3^2 \\ 2q_2q_3 + 2q_0q_1 \end{pmatrix},$$

$$\mathbf{u}_1 = \begin{pmatrix} 2q_1q_3 + 2q_0q_2 \\ 2q_2q_3 - 2q_0q_1 \\ q_0^2 - q_1^2 - q_2^2 + q_3^2 \end{pmatrix}.$$

These Euler parameters, unlike Euler angles, give a singularity-free description of arbitrary rotations in space and are therefore convenient for numerical computations. The kinematics equations are obtained by differentiating the above vectors and using Eq. (12.2.1):

$$\frac{d}{ds} \begin{pmatrix} q_0 \\ q_1 \\ q_2 \\ q_3 \end{pmatrix} = \frac{1}{2} \begin{pmatrix} 0 & -\omega_1 & -\omega_2 & -\omega_3 \\ \omega_1 & 0 & \omega_3 & -\omega_2 \\ \omega_2 & -\omega_3 & 0 & \omega_1 \\ \omega_3 & \omega_2 & -\omega_1 & 0 \end{pmatrix} \begin{pmatrix} q_0 \\ q_1 \\ q_2 \\ q_3 \end{pmatrix}, \quad (12.2.23)$$

where we recall from Eq. (12.2.8) that $\omega_1 = (\omega_3 - \frac{1}{\Delta}) \tan \eta$. It is straightforward to verify that $\mathbf{q} \cdot \mathbf{q}$ is a first integral of this system of equations. To find the centreline \mathbf{r}_1 we solve Eq. (12.2.23) in conjunction with the equation $\mathbf{r}'_1 = \mathbf{t}_1$. The second centreline is then given by $\mathbf{r}_2 = \mathbf{r}_1 + \Delta \mathbf{d}_1$.

12.3 Numerical solution

In this section we present results obtained by numerically solving boundary-value problems for the standard 2-braid equations developed in Section 2 using the continuation and bifurcation code AUTO [3]. AUTO solves ODEs using collocation and uses pseudo-arclength continuation to advance solutions as a control (or bifurcation) parameter is incremented. The code is also able to detect pitchfork or other bifurcation points along a solution branch where this branch intersects another solution branch and to switch to and compute this second branch. In this work we choose the strand torque as a bifurcation parameter.

Here we consider only the closed braid problem where the two rods form a torus knot or link. We define a linking number to distinguish between topologically different types of such 2-braid solutions by following Fuller's extension of the concept of a linking number to a (not necessarily closed) ribbon [4]. By a ribbon is here meant a curve with a field of normal vectors of constant length. First note that the contact curve of our knot $\frac{1}{2}[\mathbf{r}_1(s) + \mathbf{r}_2(s)] = \mathbf{r}_1(s) + \frac{\Delta}{2}\mathbf{d}_1(s)$, $s \in [0, L]$, is a (smoothly) closed curve and the director $\frac{\Delta}{2}\mathbf{d}_1(s)$ is an orthogonal vector defined for all $s \in [0, L]$. It therefore forms a non-closed ribbon. The linking number of this ribbon is defined as $\mathcal{L}k = \mathcal{J}w + \mathcal{W}r$,

where $\mathcal{W}r$ is the writhing number of the contact curve and $\mathcal{T}w = \frac{1}{2\pi} \int_0^L tw(s) ds$ is the total twist (the twisting number) of the braid with twist rate tw . To have a closed single centreline, $\mathcal{L}k$ has to be semi-integer, $\mathcal{L}k = n/2$, $n \in \mathbb{Z}$. Alternatively, if we think of the ribbon as extended in both $\pm \frac{1}{2} \mathbf{d}_1$ directions, we may say that, for our knots, this ribbon is one-sided (like a Möbius strip [10]) and its edge (given by the centreline of the rod) is a single knotted curve.

We start from an analytical solution (two linked equidistant circular rings) and perform continuations mimicking the cutting, twisting and resealing of the rings to obtain different torus knots (and links) [12] and eventually, after torsionally buckling these knots/links, cable knots/links. The braid axis (contact curve) of this starting solution is an unknot. We compute solutions with different linking numbers for which we derive boundary conditions that ensure smooth closure of the braid into a knot (for semi-integer linking number of the braid) or a link (for integer linking numbers).

In addition to the 13-dimensional system of ODEs derived in Section 12.2.2 we solve the 7 kinematics equations for \mathbf{q} and \mathbf{r}_1 of Section 12.2.3, so as to be able to apply displacement boundary conditions and plot solution shapes, and Eq. (12.2.6) to compute the second arclength. Integration of this last equation allows us to impose the total-length constraint $L_{\text{tot}} := L + L_2 = \text{const.}$, the natural constraint to consider for knot solutions. Since $\mathbf{q} \cdot \mathbf{q}$ is an integral of the kinematics equations, the quaternion normalisation condition $|\mathbf{q}| = 1$ can simply be imposed by choosing boundary conditions for the q_i that satisfy it.

All numerical runs are for elastic parameters $B_1 = B_2 = 1$, $C_1/B_1 = C_2/B_2 = 1/(1 + \nu)$, where Poisson's ratio $\nu = 0.3$, and in all cases we set $\omega_{01} = \omega_{02} = 0$. Given a solution of the 21D system of ODEs we can compute other properties such as the normal contact pressure p or the curvature κ_c of the contact curve (see details in [12]). Here we make the assumption of frictionless hardcore contact in which the only distributed force acting between the two contacting strands is the normal pressure directed along the chord vector \mathbf{d}_1 . First integrals are monitored throughout to keep track of the numerical accuracy of solutions.

12.3.1 Torus knots

12.3.1.1 Boundary conditions

To compute knot solutions of total length L_{tot} we apply the following boundary conditions

$$\begin{aligned}
x_1(0) &= 0, & (12.3.1) & & x_1(L) - x_1(0) &= \Delta, & (12.3.13) \\
y_1(0) &= 0, & (12.3.2) & & y_1(L) &= 0, & (12.3.14) \\
z_1(0) &= 0, & (12.3.3) & & z_1(L) &= 0, & (12.3.15) \\
q_0(0) &= 0, & (12.3.4) & & q_0(L) &= q_3(L), & (12.3.16) \\
q_1(0) &= -1/\sqrt{2}, & (12.3.5) & & q_1(L) &= -q_2(L), & (12.3.17) \\
q_2(0) &= -1/\sqrt{2}, & (12.3.6) & & 4q_0(L)q_1(L) &= \sin \eta(L), & (12.3.18) \\
q_3(0) &= 0, & (12.3.7) & & \eta(L) &= \eta(0), & (12.3.19) \\
\xi_1(0) &= 0, & (12.3.8) & & [M_2(0) - B_1\omega_2(0)]/B_2 &= -\omega_2(L), & (12.3.20) \\
\xi_2(0) &= 0, & (12.3.9) & & (1 - \Delta\omega_3(0))/\cos \eta(0) &= \cos \eta(L)/(1 - \Delta\omega_3(L)), & (12.3.21) \\
T_1(0) &= t_{10}, & (12.3.10) & & \sigma(L) &= L_2, & (12.3.22) \\
T_2(0) &= t_{20}, & (12.3.11) & & L + L_2 &= L_{\text{tot}}, & (12.3.23) \\
\sigma(0) &= 0, & (12.3.12) & & & &
\end{aligned}$$

where t_{10} and t_{20} are constants. Since for a knot the two strands are part of a single closed rod, it only makes good sense to take $t_{20} = -t_{10}$ and also $B_2 = B_1$, $C_2 = C_1$.

Conditions Eqs. (12.3.1)–(12.3.7), (12.3.13)–(12.3.21) ensure smooth closure of the braid into a doubly-covered ring, smooth here meaning continuity up to second derivatives of \mathbf{r}_i , i.e., curvatures. Conditions Eqs. (12.3.13)–(12.3.15) place the end of the first centreline \mathbf{r}_1 at the beginning of the second centreline \mathbf{r}_2 , both strands thus forming a single closed rod. Conditions Eqs. (12.3.16) and (12.3.17) imply $\mathbf{d}_1(L) = -\mathbf{d}_1(0)$. Condition Eq. (12.3.18) guarantees that $\mathbf{t}_1(L)$ makes an angle $\eta(L)$ with $\mathbf{t}_1(0)$ of the same strand. Together with condition Eq. (12.3.19) this ensures matching of the tangents: the tangent at $s = L$ of the first strand aligns with the tangent at $s = 0$ of the second strand, and vice versa. Conditions Eqs. (12.3.19)–(12.3.21) are equivalent to $\Omega_1(0)/\sigma'(0) = \omega_1(L)$, $\Omega_2(0)/\sigma'(0) = -\omega_2(L)$ and $\Omega_3(0)/\sigma'(0) = -\omega_3(L)$, which ensure that the curvatures at the end of the first strand match the curvatures at the beginning of the second strand.

The total number of boundary conditions is 23 and the three free parameters required for solution branches are L , L_2 and t_{10} . Note that the material frames of these knot solutions will in general not be closed. This is not different from similar studies of closed single rods (see, e.g., [9, 7]). Material closure requires $\xi_1(0) + \xi_2(L) = \pi \pmod{2\pi}$ and can be achieved by inserting the right amount of twist by adjusting t_{10} ($= -t_{20}$).

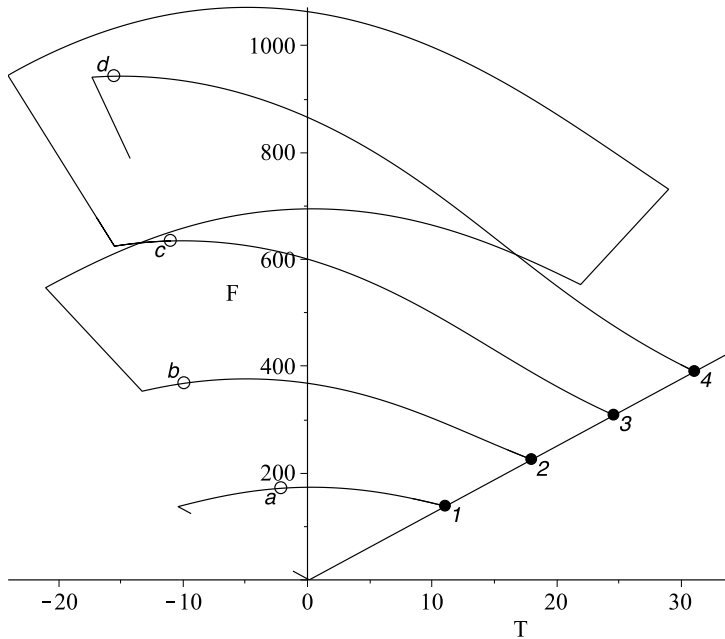


Fig. 12.2: Partial bifurcation diagram for the $(7, 2)$ torus knot with the first four bifurcation points (marked with solid black circles) and bifurcating branches. $\Delta = 0.0051364907419$, $L_{\text{tot}} = 1.98889$. Empty circles mark particular cable knots whose shapes are shown separately in the following figures.

12.3.1.2 Examples of cable knots

Cable knots [2] can be obtained by inserting twist into the torus knots computed using the above boundary conditions thereby forcing them to buckle (bifurcate). The bifurcation diagram in Fig. 12.2 shows how cable knots appear along bifurcating solution branches. The figure presents a (T, F) diagram, where $T := t_{10} = T_1 = -T_2$ is the common strand torque and $F = |\mathbf{F}|$ is the magnitude of the constant braid force as a characteristic solution measure. The diagram is for the (right-handed) $(7, 2)$ torus knot. The trivial branch, representing unbuckled knots with unknotted braid axis, makes an infinite v-shaped curve (only part of this branch, marked 1 – 2 – 3 – 4, is shown in Fig. 12.2). The solutions along the v-branch are D_7 -symmetric with the central axis aligned with the force vector. We shall refer to them as ‘flat’ solutions because in many ways they behave like twisted planar circular isotropic rods (which have linear F - T relationship for branches of planar equilibria [7]). This is despite the fact that neither the contact curve of the braid nor the centreline of the rod is a plane curve.

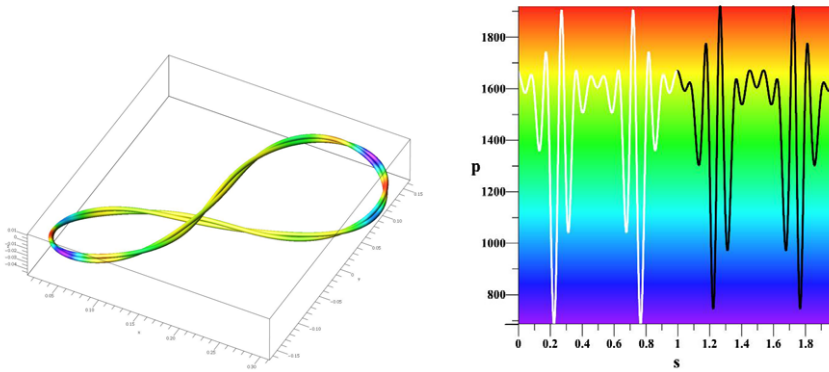


Fig. 12.3: Figure-8-shaped $(11, 2)$ torus knot. $T = -2.10752$, $F = 171.50131$ ((a) in Fig. 12.2). $\Delta = 0.0051364907419$, $L_{\text{tot}} = 1.98889$.

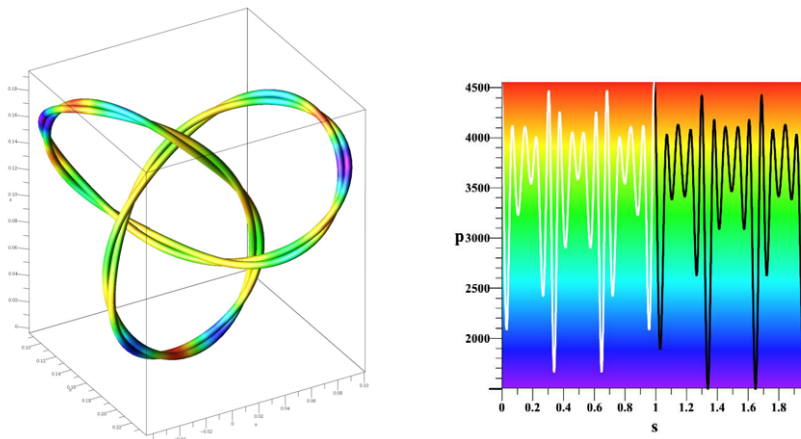


Fig. 12.4: Buckled right-handed cable knot formed by knotting a right-handed $(13, 2)$ torus knot into a right-handed trefoil. $T = -9.89105$, $F = 368.075$ ((b) in Fig. 12.2). $\Delta = 0.0051364907419$, $L_{\text{tot}} = 1.98889$.

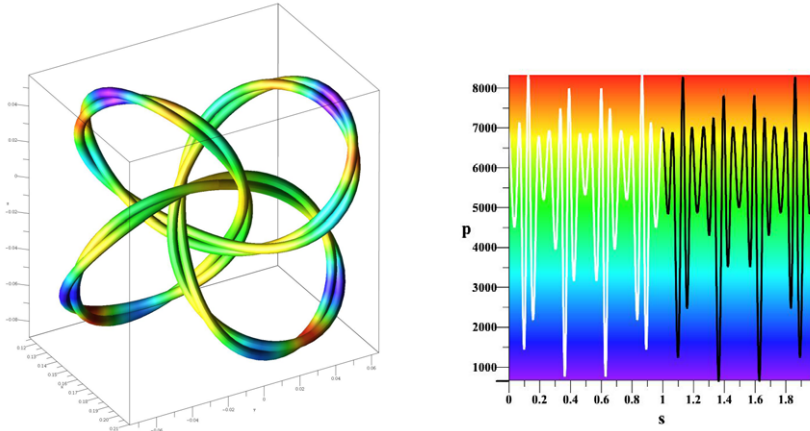


Fig. 12.5: Buckled right-handed cable knot formed by knotting a right-handed (7, 2) torus knot into a right-handed (4, 3) torus knot. $T = -10.97932$, $F = 634.5698$ ((c) in Fig. 12.2). $\Delta = 0.0051364907419$, $L_{\text{tot}} = 1.98889$.

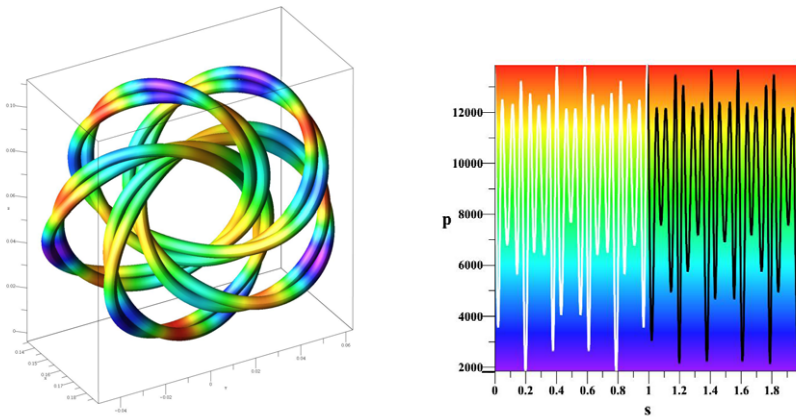


Fig. 12.6: Buckled right-handed cable knot formed by knotting a right-handed (7, 2) torus knot into a right-handed (5, 4) torus knot. $T = -15.51471$, $F = 942.989$ ((d) in Fig. 12.2). $\Delta = 0.0051364907419$, $L_{\text{tot}} = 1.98889$.

There exist critical torque levels T , corresponding to bifurcation points 1, 2, 3, 4, . . . in the diagram, where new branches of more warped (buckled) solutions begin. This sequence of buckling modes is again similar to the behaviour of a single closed elastic rod (cf. Fig. 3 in [7]). Figure 12.2 shows branches for the first four bifurcating modes, with the bifurcation points marked by solid black circles. As we move further away from the right side of the v -branch, shapes become more warped and at some point begin to self-overlap. The braid axis exhibits a multiple self-intersection depending on the mode, becoming knotted for modes 2 and higher. Continuing along the branch we come to an interval where the shape becomes free of self-overlapping, see points a , b , c and d in Fig. 12.2 (this may not happen if the rod is too thick). These solutions are cable knots, examples of which are shown in Figs. 12.3–12.6.

The braid axis of the first mode shape in Fig. 12.3, going through a single figure-8-type self-intersection, remains unknotted; we present it here only for completeness of the picture. We see that the right-handed $(7, 2)$ torus knot becomes a $(11, 2)$ torus knot after self-crossing. The linking number of the shape shown is $3.5 + 2 = 5.5$. Each of the curves corresponding to the various modes ends at another v -branch (only parts of which are shown in Fig. 12.2). These represent multi-covered ‘flat’ solutions also having their own bifurcation points. As they are self-overlapping for modes higher than one, we do not explore them further.

All solutions in Figs. 12.3–12.6 have been computed by continuation from the $(7, 2)$ torus knot and have the same total length $L_{\text{tot}} (= 1.98889)$. (The shape in Fig. 12.6 has a small overlapping domain because the chosen value of Δ is just too large.) In particular, the trefoil cable in Fig. 12.4 is obtained by continuation of a right-handed $(7, 2)$ torus knot that after a triple self-crossing becomes a $(13, 2)$ torus knot tied into a right-handed trefoil. Thus, the torus knot (inside the tubular neighbourhood of the companion trefoil knot) has linking number $3.5 + 3 = 6.5$. The corresponding linking numbers for the cable knots in Figs. 12.5 and 12.6 are 7.5 and 8.5, respectively.

The set of all knot solutions breaks down into two components. A disjoint bifurcation diagram, the mirror image of the present diagram under reflection in the F -axis, consists of all solutions connected to the left-handed $(7, 2)$ torus knot (hence, the left-handed trefoil).

The contact pressure profile is drawn in white for $s \in [0, L]$ and in black for $s \in [L, L_{\text{tot}}]$ in Figs. 12.3–12.6. This allows one to see the differences for both contacting strands. The profile differences are larger for thicker rods. We observe that for all solutions shown the contact pressure is non-negative and increases with the mode.

12.3.2 Torus links

12.3.2.1 Boundary conditions

To compute link solutions we apply the following boundary conditions:

$$x_1(0) = 0, \quad (12.3.24)$$

$$y_1(0) = 0, \quad (12.3.25)$$

$$z_1(0) = 0, \quad (12.3.26)$$

$$q_0(0) = 0, \quad (12.3.27)$$

$$q_1(0) = -1/\sqrt{2}, \quad (12.3.28)$$

$$q_2(0) = -1/\sqrt{2}, \quad (12.3.29)$$

$$q_3(0) = 0, \quad (12.3.30)$$

$$\xi_1(0) = 0, \quad (12.3.31)$$

$$\xi_2(0) = 0, \quad (12.3.32)$$

$$T_1(0) = t_{10}, \quad (12.3.33)$$

$$T_2(0) = t_{20}, \quad (12.3.34)$$

$$\sigma(0) = 0, \quad (12.3.35)$$

$$x_1(L) = x_1(0), \quad (12.3.36)$$

$$y_1(L) = y_1(0), \quad (12.3.37)$$

$$z_1(L) = z_1(0), \quad (12.3.38)$$

$$q_0(L) = q_3(L), \quad (12.3.39)$$

$$q_1(L) = q_2(L), \quad (12.3.40)$$

$$q_0(L) + q_1(L) = -\sin(\Phi/2 - \pi/4), \quad (12.3.41)$$

$$\omega_2(0) \text{ fixed}, \quad (12.3.42)$$

$$\omega_2(L) = \omega_2(0) \cos \Phi + \omega_3(0) \sin \Phi, \quad (12.3.43)$$

$$\sigma(L) = L_2, \quad (12.3.44)$$

where t_{10} and t_{20} are constants and $\omega_2(0)$ is fixed at whatever value the starting solution has.

The q_i conditions at $s = 0$ imply that \mathbf{t}_1 is aligned with the y axis, \mathbf{d}_1 is aligned with the x axis and \mathbf{u}_1 is aligned with the $-z$ axis. Conditions Eqs. (12.3.39) and (12.3.40) ensure alignment of the tangents $\mathbf{t}_1(0)$ and $\mathbf{t}_1(L)$. Φ is the angle between $\mathbf{d}_1(0)$ and $\mathbf{d}_1(L)$ in the plane normal to these tangents. Closed links have $\Phi = \pm 2\pi n$, where n is a non-negative integer. By using parameter continuation in Φ solutions with different linking number $\mathcal{L}k = \pm n$ may be obtained, positive linking numbers corresponding to right-handed and negative linking numbers corresponding to left-handed links.

This gives a total of 21 conditions for a 21-dimensional system of equations. To compute branches of solutions for a given link we may vary one of the parameters, for example t_{10} or Δ . For equal twisting of the two strands (in the same direction), t_{20} may be taken equal to $-t_{10}$. Note that closure of the material frames of these link solutions requires $\xi_i(L) = \xi_i(0) \pmod{2\pi}$, $i = 1, 2$, which will not in general be satisfied.

12.3.2.2 Examples of cable links

Similar to how we computed cable knots, we first compute a trivial branch of ‘flat’ torus links with unknotted contact curve. Then, following the branches of post-buckled solutions of different modes, we observe knotting of the braid axis by multiple self-intersection, thus forming what we call cable links. Figs. 12.7–12.9 present, respectively, mode-2, -3 and -4 cable links with equal-length components ($L_1 = L_2$). The

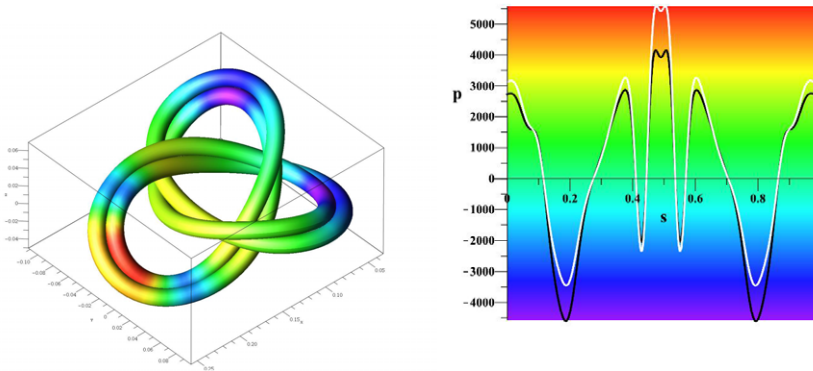


Fig. 12.7: Buckled right-handed cable link formed by knotting a left-handed (6, 2) torus link into a right-handed (3, 2) torus knot. $T_1 = -T_2 = -11.46623$, $F = 364.061$, $\Delta = 0.016016913268$, $L_1 = L_2 = 1$.

shape in Fig. 12.7 is obtained by taking a left-handed ‘flat’ torus link (6, 2) and following the second bifurcating branch. After self-intersection, the axis of the braid becomes a right-handed trefoil (a companion knot). As can be verified directly from the image in Fig. 12.7, the two strands are not linked inside a tube imagined around the knotted braid axis. The linking number of this link equals 3. A similar procedure applied to a ‘flat’ torus link emanating from a third mode bifurcation, results in a cable of a right-handed (4, 3) torus knot (Fig. 12.8). The two components form a 1-link inside an imaginary tube around the knotted axis of the braid. The linking number of the link is 9. The fourth mode bifurcating branch of the initial ‘flat’ torus link (10, 2) leads to a cable of a right-handed (5, 4) torus knot (Fig. 12.9) and the two strands are not linked inside the knotted tube. The linking number of this link is 15.

In all Figs. 12.7–12.9, the contact pressure profiles are displayed as functions of arclength s along the first strand, in white for the pressure on the first strand and in black for the pressure on the second strand. Note that for all three examples the contact pressure changes sign, which means that the physical realisation would require a mechanism (e.g., glue or a clamp) to keep the strands together.

12.4 Concluding remarks

We have shown how the simplest cable knots and links emerge as equilibrium configurations of closed braids made of two equidistant elastic strands. Cable links present an obvious generalisation of cable knots when there is more than one component. A

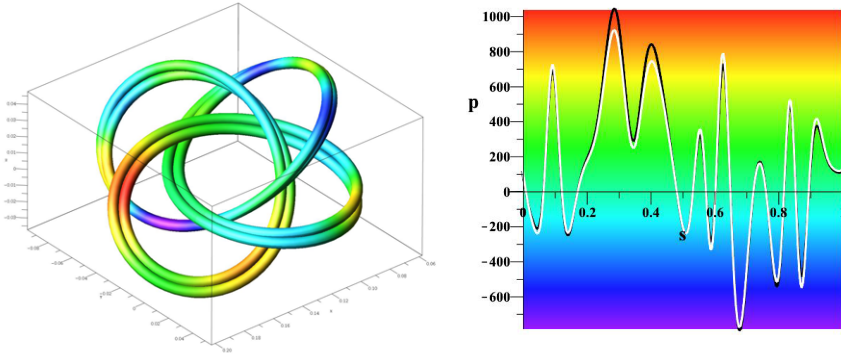


Fig. 12.8: A cable of a right-handed (4, 3) torus knot. $T_1 = -T_2 = -14.49330$, $F = 633.545$, $\Delta = 0.006$, $L_1 = L_2 = 1$.

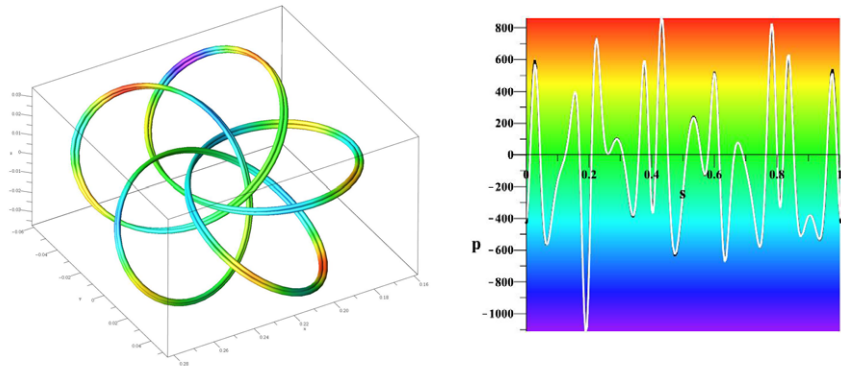


Fig. 12.9: Buckled right-handed cable link formed by knotting a left-handed (10, 2) torus link into a right-handed (5, 4) torus knot. $T_1 = -T_2 = -14.63829$, $F = 946.310$, $\Delta = 0.002$, $L_1 = L_2 = 1$.

further natural extension of this mechanical problem would be to increase the number of strands in the braid, which requires the development of a multi-strand elastic braid theory. Although this calls for a more sophisticated technique to account for equidistant constraints on multiple strands, we do not expect a significant difference in qualitative geometrical properties of mechanical equilibrium solutions for thin elastic rods.

Bibliography

- [1] S. S. Antman. *Nonlinear Problems of Elasticity*. Springer, 2nd edition, 2005.
- [2] G. Burde and H. Zieschang. *Knots*. de Gruyter, Berlin, 2nd edition, 2002.
- [3] Doedel, E. et al. AUTO: Software for continuation and bifurcation problems in ordinary differential equations. User's manual, Concordia University, Montreal, Canada, 2007.
- [4] F. B. Fuller. Decomposition of the linking number of a closed ribbon: A problem from molecular biology. *Proceedings of the National Academy of Sciences of the United States of America*, 75(8):3557–3561, 1978.
- [5] O. Gonzalez, J. H. Maddocks, F. Schuricht, and H. von der Mosel. Global curvature and self-contact of nonlinearly elastic curves and rods. *Calculus of Variations and Partial Differential Equations*, 14:29–68, 2002.
- [6] A. J. Hanson. Quaternion Frenet frames: making optimal tubes and ribbons from curves. Technical report TR407, Indiana Univ., Dept. of Computer Science, 1994.
- [7] K. A. Hoffman. Stability results for constrained calculus of variations problems: an analysis of the twisted elastic loop. *Proceedings of the Royal Society A: Mathematical, Physical and Engineering Science*, 461(2057):1357–1381, 2005.
- [8] F. Schuricht and H. von der Mosel. Euler-Lagrange equations for nonlinearly elastic rods with self-contact. *Archive for Rational Mechanics and Analysis*, 168:35–82, 2003.
- [9] E. L. Starostin. Three-dimensional shapes of looped DNA. *Meccanica*, 31:235–271, 1996.
- [10] E. L. Starostin and G. H. M. van der Heijden. The shape of a Möbius strip. *Nature Materials*, 6(8):563–567, 2007.
- [11] E. L. Starostin and G. H. M. van der Heijden. Force and moment balance equations for geometric variational problems on curves. *Physical Review E*, 79(6):066602, Jun 2009.
- [12] E. L. Starostin and G. H. M. van der Heijden. Theory of equilibria of elastic 2-braids with interstrand interaction. *Journal of the Mechanics and Physics of Solids*, 64:83–132, 2014.
- [13] G. H. M. van der Heijden, M. A. Peletier, and R. Planqué. Self-contact for rods on cylinders. *Archive for Rational Mechanics and Analysis*, 182:471–511, 2006.